PHOTONICS Research

Over 255 mW single-frequency fiber laser with high slope efficiency and power stability based on an ultrashort Yb-doped crystal-derived silica fiber

YING WAN,[1] JIANXIANG WEN,[1,*] CHEN JIANG,[1] FENGZAI TANG,[2,4] JING WEN,[3] SUJUAN HUANG,[1] FUFEI PANG,[1] AND TINGYUN WANG[1,5]

[1]Key Laboratory of Specialty Fiber Optics and Optical Access Networks, Joint International Research Laboratory of Specialty Fiber Optics and Advanced Communication, School of Communication and Information Engineering, Shanghai University, Shanghai 200444, China
[2]WMG, University of Warwick, Coventry CV4 7AL, UK
[3]Optoelectronics Research Centre, University of Southampton, Southampton SO17 1BJ, UK
[4]e-mail: fengzai.Tang@warwick.ac.uk
[5]e-mail: tywang@shu.edu.cn
*Corresponding author: wenjx@shu.edu.cn

Received 6 January 2021; revised 8 February 2021; accepted 11 February 2021; posted 12 February 2021 (Doc. ID 419178); published 14 April 2021

A single-frequency distributed Bragg reflector (DBR) fiber laser at 1030 nm has been demonstrated using a 0.7 cm long homemade Yb:YAG crystal-derived silica fiber (YCDSF). The absorption and emission cross sections of the YCDSF are 4.93×10^{-20} cm^2 at 980 nm and 1.1×10^{-20} cm^2 at 1030 nm. Using this gain fiber, an over 255 mW continuous-wave lasing in the constructed laser has been obtained at single transverse and longitudinal mode operation. The slope efficiency and the pump threshold of the fiber laser were up to ∼35% and as low as 25 mW, respectively. The fiber laser also demonstrated an optical signal-to-noise ratio of 79 dB and a beam quality factor of 1.016 in two orthogonal directions. Its power fluctuation at 210.5 mW was less than 0.85% of the average power within 13 h. Moreover, the relative intensity noise and linewidth of the laser are also investigated at the different pump powers. The results indicate that the single-frequency DBR fiber laser has potential applications in high-quality seed sources and high-precision optical sensing.

https://doi.org/10.1364/PRJ.419178

1. INTRODUCTION

Single-frequency fiber lasers (SFFLs) have attracted considerable attention because of their remarkable narrow linewidth, low noise, high stability, and compact all-fiber configuration. These merits have inevitably driven the increasing applications of SFFLs in the generation of optical frequency combs and in nonlinear frequency conversion, gravitational wave detection, and coherent beam combining [1–4]. The lasing performance of SFFLs, such as slope efficiency, maximum output power, linewidth, and stability, is strongly influenced by the cavity configuration and the properties of the gain fiber. In the cavity design, various approaches have been utilized to accomplish single-longitudinal-mode (SLM) operation, such as distributed Bragg reflectors (DBRs) [5], a distributed feedback (DFB) configuration [6], a long linear cavity [7], and a traveling-wave ring cavity [8]. In the last two designs, the cavity length on the order of meters has to be applied, together with a narrow filter, in order to maintain the SLM operation, whereas the DBR and DFB configurations have cavity lengths of only several centimeters. Such ultrashort cavity configurations allow them to obtain a longitudinal mode interval of up to several gigahertz (GHz) and achieve a stable SLM operation more easily. In general, the DFB cavity is formed by writing a pair of fiber Bragg gratings (FBGs) on the gain fiber, which necessarily imposes a high requirement on the grating writing technology. On the contrary, building the DBR cavity is relatively easy, and the resultant fiber laser has a more robust, compact structure and a high slope efficiency [5]. As far as the gain fiber is concerned, recent decades have witnessed great efforts in developing novel gain fibers to realize high-efficiency SFFLs, such as highly rare-earth-doped phosphate fibers, tellurite-based fibers, and crystal-derived silica fibers [9–14]. Among these gain fibers, yttrium aluminum garnet (YAG) crystal-derived silica fibers are of great interest. Because of their excellent physical and chemical properties, the derived fibers are compatible with commercialized silica-based fibers and have the capability of doping a high level of rare-earth ions [15–18]. On the other hand, optical fiber fabrication technology has progressed rapidly in the recent two decades, providing an opportunity for the development of high-quality gain fibers. For instance, the melt-in-tube method has contributed greatly to the development of YAG crystal-derived silica optical fibers [19,20], which can be used as promising gain fiber materials in single-frequency DBR fiber lasers.

In 2012, the Yb-doped YAG crystal-derived silica fiber (YCDSF) was investigated as a heavily doped gain medium for fiber-amplifier applications [15], and the obtained fibers showed a higher Yb doping level with a greater uniformity over conventional Yb-doped aluminosilicates. Moreover, it is also expected that the YCDSF-based fiber lasers could have a better performance in output power over the silica-based fiber lasers due to the increased threshold of the stimulated Brillouin scattering [21]. Since then, a number of studies on high-power fiber lasers and SFFLs have been carried out based on the developed YCDSFs [13,22–25]. To date, the maximum output power of the SFFLs can be up to 110 mW, and the associated slope efficiency is 18.5% [13]. The improvement of the SFFL performance is deemed to go along with the development of high-quality gain fibers. Previously, we fabricated a high-gain YCDSF based on the melt-in-tube method on a CO_2 laser-heated drawing tower and built a DBR fiber laser based on a 1.5 cm long YCDSF [26]. The technique has a much shorter hot zone compared to the traditional graphite-heated fiber drawing method [13,26,27], i.e., about 13 mm versus 40 mm. As a consequence, it may suppress silica diffusion from the cladding region into the YAG crystal core, sustaining a high Yb doping level in the resultant YCDSF. The fiber laser showed an optimum performance with a maximum output power of 360 mW and a slope efficiency of 50.5%. However, it did not operate at a single frequency.

In this work, single transverse and longitudinal mode operation at 1030 nm has been accomplished through innovatively incorporating an ultrashort, highly efficient YCDSF into an all-fiber DBR cavity with the aid of theoretical calculations. A significant breakthrough has been made in the maximum output powers and the slope efficiency through the built DBR laser cavity containing a 0.7 cm long YCDSF. The absorption and emission cross sections of the YCDSF are calculated and analyzed as well as the gain cross section. The lasing characteristics of the SFFL have been systematically investigated in terms of its longitudinal mode operation, slope efficiency, output spectrum, power stability, beam quality, and noise. The established approach could provide insight into the study of a range of high-efficiency SFFLs doped with other rare-earth ions at other operating wavelengths.

2. Yb:YAG CRYSTAL-DERIVED SILICA FIBER AND THE LASER SETUP

The YCDSFs were fabricated using the melt-in-tube method on a CO_2 laser-heated drawing tower, and the used fiber preform had a YAG crystal core and a silica cladding as schematically illustrated in Fig. 1(a). In this figure, the side and cross-sectional views of the YCDSFs are also presented as the inset optical images. In general, no apparent defects, such as bubbles and cracks, were observed in the fibers. The X-ray diffraction (XRD) analysis of the Yb:YAG crystal rod and the fiber cores was conducted using a Rigaku D/max-2500 X-ray diffractometer (Rigaku Co., Japan). As shown in Fig. 1(b), the sharp

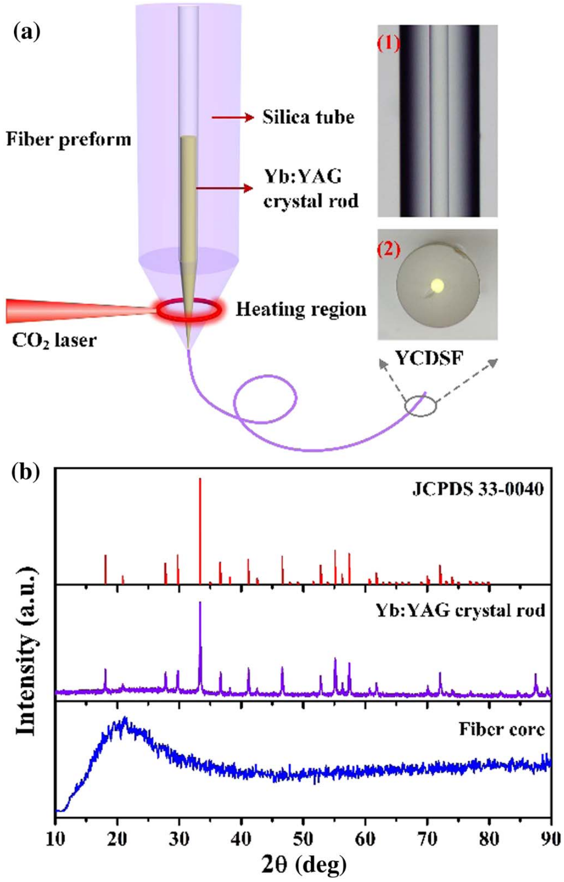

Fig. 1. (a) Schematic diagram of YCDSF fabrication using the preform with a YAG crystal core and a silica cladding, where the insets are the optical images of the (1) side view and (2) cross-sectional view of the YCDSF; (b) XRD analysis of the YAG crystal rod and the fiber cores.

diffraction peaks of the Yb:YAG crystal rod fit well with those of the YAG crystal (JCPDS 33-0040). No sharp diffraction peaks can be found on the measurement of fiber cores, and the exhibited large broad peak centered at 22 deg can be attributed to amorphous silica. The result indicates the amorphous nature of the YCDSF cores.

From our previous study [26], it is known that the Yb ion concentration in the YCDSF is approximately 5.66% (mass fraction), and the fiber has an absorption coefficient of 32 dB/cm at 980 nm. The YCDSF has also a figure of merit of the unsaturated absorption of 93% and a gain per unit length of 4.4 dB/cm at 1030 nm. More details of the fiber properties can be found in Ref. [26]. The absorption, emission, and gain cross sections (δ_{abs}, δ_{emi} and δ_{gain}) of the YCDSFs were also investigated, and the results are depicted in Fig. 2. It is found that the δ_{abs} at 980 nm is 4.93×10^{-20} cm^2, and the δ_{emi} at 1030 nm is 1.1×10^{-20} cm^2 [Fig. 2(a)]. Based on the δ_{abs} and δ_{emi} of the YCDSF, its δ_{gain} can be evaluated by the following equation [28]:

$$\delta_{gain}(\lambda) = P\delta_{emi}(\lambda) - (1 - P)\delta_{abs}(\lambda), \quad (1)$$

where P is the normalized population of the upper laser level. The calculated δ_{gain} of the YCDSF for P ranging from 0 to 1

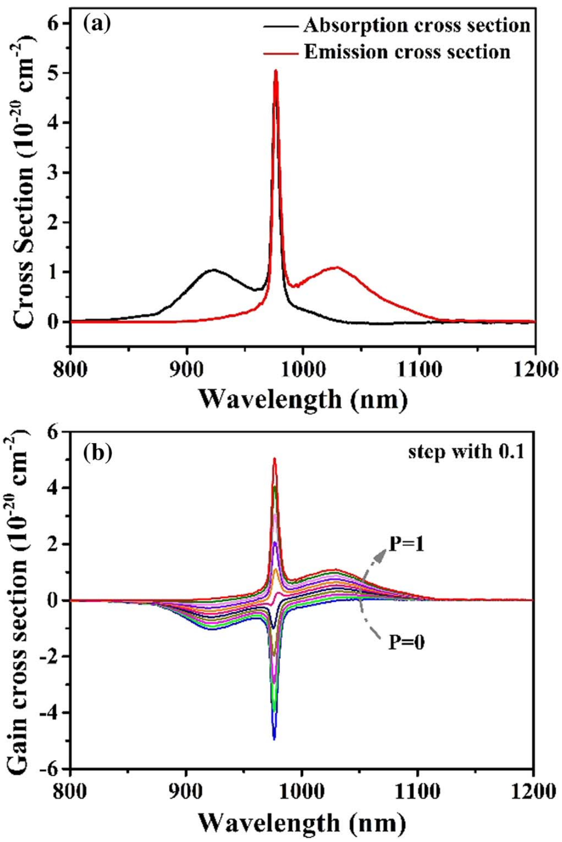

Fig. 2. (a) Absorption and emission cross sections of the YCDSF; (b) gain cross section of the YCDSF.

with a step of 0.1 are shown in Fig. 2(b). Two prominent gain peaks are observed whose central wavelengths are at 980 nm and 1030 nm, respectively. According to the calculated results, a positive gain cross section at 1030 nm can be achieved when the P value is larger than 0.1. At such conditions, the YCDSF-based fiber lasers or amplifiers at 1030 nm could have a high conversion efficiency [29]. Based on the obtained absorption and emission cross-section spectra of the YCDSF, the key parameters indicating the lasing performance have been evaluated using the methods in Ref. [30], i.e., the minimum fraction of Yb ions ($\beta_{\min}$), the pump saturation (I_{sat}), the minimum absorbed pump intensity ($I_{\min}$), and the systematical factor (SF), and the estimated values are 0.027, 8.338 kW/cm^2, 0.225 kW/cm^2, and 2.420, correspondingly. This suggests that the laser based on the fabricated YCDSFs would render a better performance in comparison with those using aluminosilicate or phosphate glass fibers [31,32].

Figure 3 illustrates the setup of single-frequency DBR fiber laser system and its associated measurement system, in which a backward pump scheme is utilized. The laser system is composed of a single-mode 980/1030 nm wavelength-division multiplexer (WDM) and a pair of FBGs. The WDM was used to input the pump light at 980 nm and output the lasing light at 1030 nm simultaneously. A 980 nm laser diode (LD) having the maximum output power of 965 mW acted as the pump light source. A short section of the YCDSF (0.7 cm) was

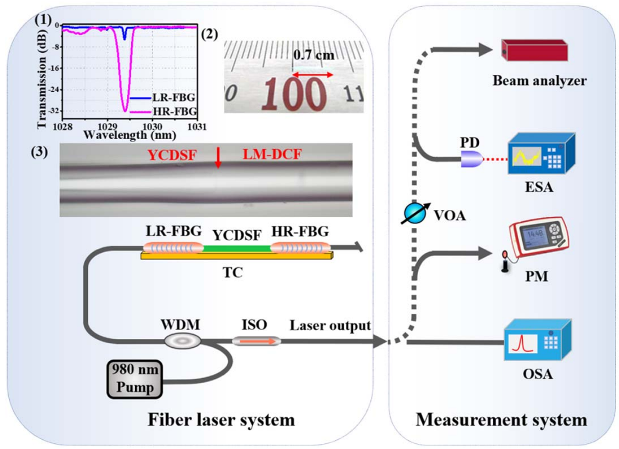

Fig. 3. Setup of the DBR SFFL based on a 0.7 cm long YCDSF and the laser measurement system (WDM, wavelength-division multiplexer; ISO, isolator; LR-FBG, low-reflectivity fiber Bragg grating; HR-FBG, high-reflectivity fiber Bragg grating; TC, temperature controller; VOA, variable optical attenuator; OSA, optical spectrum analyzer; PM, power meter; ESA, electric spectrum analyzer; PD, photodetector).

integrated with a high-reflectivity FBG (HR-FBG) and a low-reflectivity FBG (LR-FBG), forming the DBR cavity. These three components were fusion spliced using a CO_2 laser splice machine (LZM-100, AFL Fujikura, Japan). The central wavelength of the pair of FBGs is at 1029.6 nm. The LR-FBG and HR-FBG have reflectivity of 70.0% and 99.9% respectively, and their corresponding 3 dB bandwidths are 0.05 nm and 0.35 nm according to the transmission spectra [Fig. 3(1)]. In order to match the YCDSF geometry as closely as possible, the FBGs were fabricated using a large-mode-field double-clad fiber (LM-DCF) (Nufern, Inc., USA) whose core and cladding diameters are 11.0 μm and 130.0 μm, respectively. The optical image of the fused regions between the YCDSF and the LM-DCF is shown in panel (3), Fig. 3, where no obvious cracks can be observed. In the laser system, the unidirectional transmission of lasing light was maintained by a fiber isolator (ISO), and a temperature control device was also deployed in order to achieve stable SLM operation.

In the measurement system, the laser output can be selectively connected to either an optical spectrum analyzer (OSA, AQ6370, Yokogawa, Japan), power meter (PM, PM100D, Thorlabs), electrical spectrum analyzer (ESA, Agilent), or BeamSquared system (SP920, Spiricon) depending upon the requirement. The OSA was used to characterize the spectral properties of the output lasing light, and the output power of the laser was measured by the PM. With a variable optical attenuator (VOA), the laser output was converted to the electrical signals by a photodetector (PD, 818-BB-51F, Newport), and subsequently these signals were analyzed by the ESA in terms of the longitudinal mode and noise characteristics of the fiber laser. The beam quality of the laser output was also evaluated by the BeamSquared system.

First, the longitudinal mode spacing ($\Delta\nu$) of the fiber laser has been calculated by the equation $c/2nl$, where c is the speed of light, n is the fiber refractive index, and l is the length of cavity, i.e., a sum of the effective lengths of two FBGs and the physical length of the YCDSF. According to the theoretical work by Barmenkov on a Fabry–Perot FBG cavity [33], the effective length of the FBG at the working wavelength can be written as

$$L_{\mathrm{eff}} = L\frac{\sqrt{R}}{2\operatorname{atanh}(\sqrt{R})}, \tag{2}$$

where L_{eff} is the effective length of the FBG, L is the grating physical length, and R is the reflectivity of the FBG. Figure 4(a) shows the calculated effective length of the FBG as a function of reflectivity. Based on the physical lengths of the LR-FBG and HR-FBG, i.e., 1.0 cm and 1.5 cm, respectively, in this work, the corresponding effective lengths of the two FBGs are approximately 0.35 cm and 0.25 cm. Consequently, it can be found that the calculated longitudinal mode spacing gradually decreases as the length of the YCDSF inserted into the cavity increases as shown by the red curve in Fig. 4(b).

To ensure the SLM operation, twice the longitudinal mode interval should be more than the reflection bandwidth ($\Delta\upsilon$) of the laser. It is known that the reflection bandwidth of the single-frequency DBR fiber laser is mainly determined by the LR-FBG instead of the HR-FBG. In the present work, the reflection bandwidth of the LR-FBG (0.05 nm) is equivalent to 14.15 GHz [the solid blue line in Fig. 4(b)], half of which is 7.075 GHz as designated by the blue dotted line in Fig. 4(b). This determines a critical fiber length of 0.7 cm, less than which the DBR cavity will be the SLM operation as shown in the left inset in Fig. 4(b). Otherwise, the laser would operate at the multiple longitudinal mode (MLM) state [the right inset in Fig. 4(b)], i.e., with further extending the fiber length or increasing the $\Delta\upsilon$ value.

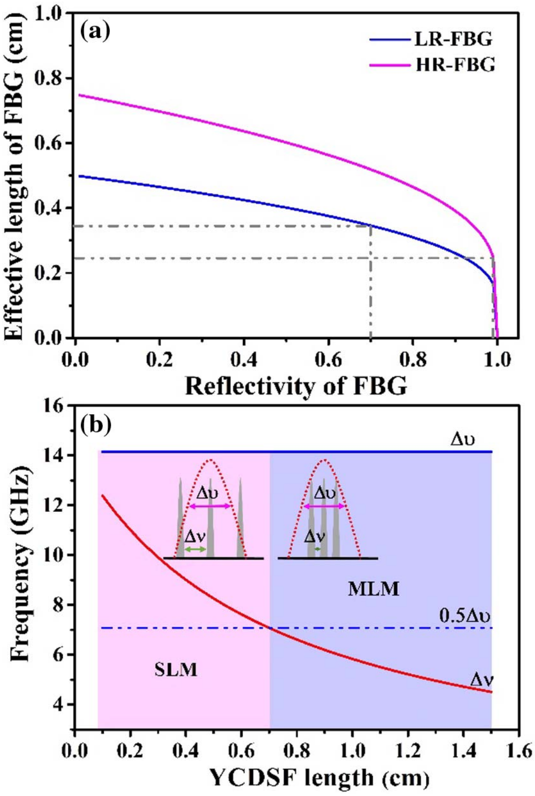

Fig. 4. (a) Calculated effective length of the HR-FBG and LR-FBG with respect to reflectivity; (b) calculated longitudinal mode spacing as a function of YCDSF length.

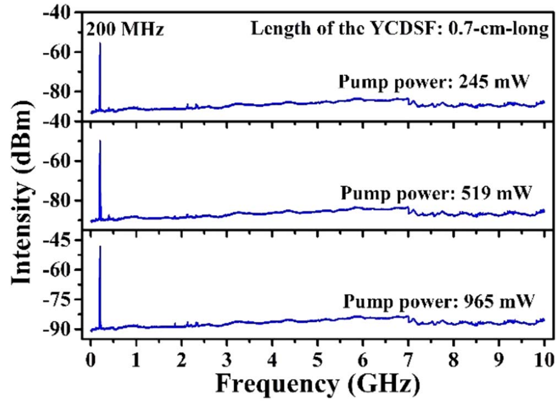

Fig. 5. Radio-frequency beating spectra of the built fiber laser with a 0.7 cm long YCDSF at different pump powers, measured by a delayed self-heterodyne measurement system.

3. EVALUATION OF THE SINGLE-FREQUENCY DBR FIBER LASER

According to the above analysis, a 0.7 cm long YCDSF has thus been unitized within the DBR cavity as depicted in panel (2), Fig. 3. The longitudinal mode characteristics of the fiber laser were assessed by a delayed self-heterodyne measurement system. The system was based on the Mach–Zehnder interference, in which a 200 MHz acoustic optical modulator (AOM) was used to generate frequency shift, and the applied ESA had a resolution bandwidth of 10 kHz. Figure 5 presents the measured radio-frequency (RF) beating spectra of the fiber laser against the frequency of 0–10 GHz at the different pump power levels. The results show a prominent beating peak at 200 MHz only, indicating a stable SLM operation obtained in the fiber laser. This result is in agreement with the theoretical work stated above.

The output characteristics of the SFFL were further analyzed as a function of the launched pump power, in terms of the output power, the absorbed pump power, and the optical-to-optical efficiency. In Fig. 6(a), the inset shows an enlarged view of the pump power ranging from 0 to 70 mW, from which a lasing threshold around 25 mW can be derived. In general, the output power as designated by the blue dot increases approximately linearly with increasing of the pump power after passing the lasing threshold, corresponding to a lasing slope efficiency of 28.2%. It reaches the maximum output power of 258 mW at the launched pump power of 965 mW. Since no saturation of output power has been observed, it implies that an even higher output power could be achieved if a higher pump power was available. On the other hand, the slope efficiency defined by the output power versus the absorbed pump power is up to 34.9% as designated by the green square in Fig. 6(a). This suggests that part of pump power was converted to the residual power in the fiber system, due probably to

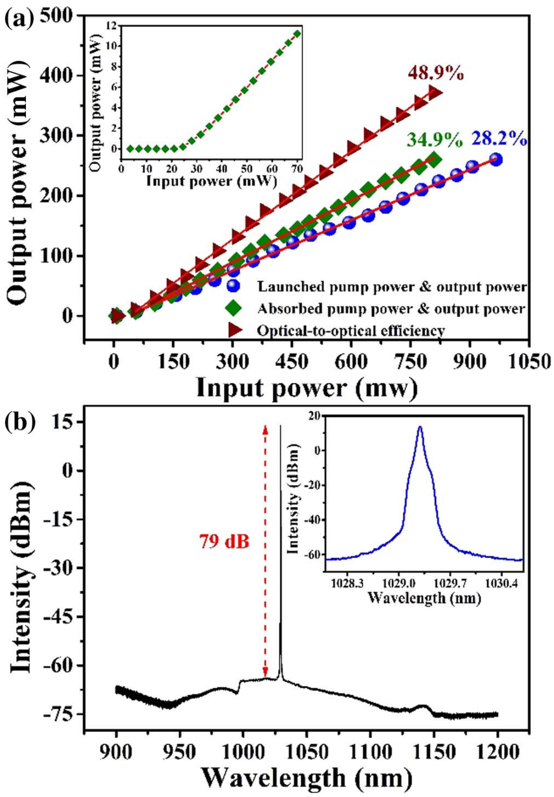

Fig. 6. (a) Output power of the SFFL as a function of pump power, and the inset shows a magnified view of the graph at a pump power range of 0 to 70 mW; (b) output spectrum of the single-frequency fiber laser under the maximum output power, and the inset is an enlarged view at the wavelengths of 1028–1031 nm.

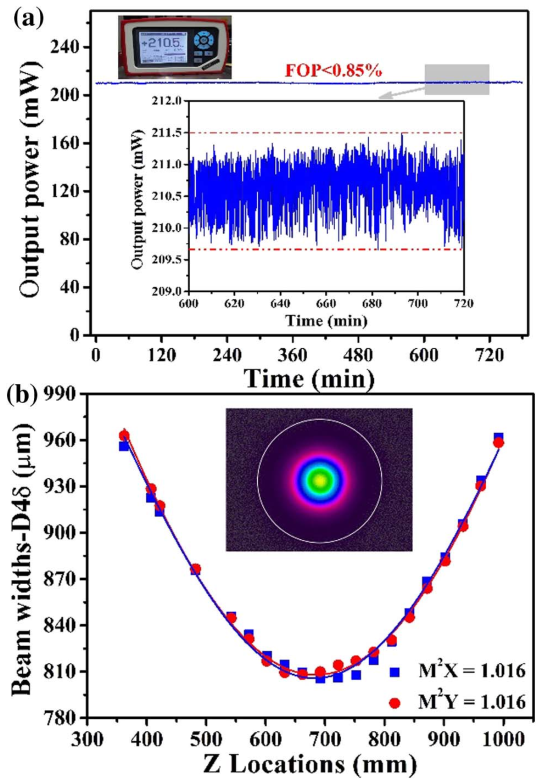

Fig. 7. (a) Laser stability record within 13 h at 210.5 mW; (b) beam quality of the fiber laser and its two-dimensional beam profile.

the ultrashort YCDSF [10,34]. Further, an optical-to-optical efficiency of 48.9% of the fiber laser [the red triangle in Fig. 6(a)] can be found after removal of the WDM loss.

At the maximum output power, the output spectrum of the SFFL was scrutinized using an OSA with the resolution of 0.02 nm. The examined spectrum ranges from 900 to 1200 nm as illustrated in Fig. 6(b), where the inset is part of magnified region of 1028 to 1031 nm. In this figure, a strong narrow-bandwidth lasing peak centered at 1029.6 nm can be seen, associated with an optical signal-to-noise ratio (OSNR) of about 79 dB and an ultranarrow bandwidth of 0.05 nm at 3 dB. Besides, there is a weak broad peak at 1025 nm, a typical amplified stimulated emission (ASE) of Yb^{3+} ions [23,26]. The highly symmetrical profile of the lasing peak and its associated ultranarrow bandwidth imply the good confinement accomplished within the laser cavity.

The power stability of the SFFL under the output power of 210.5 mW was continuously monitored for every 1 s over 13 h using a PM as shown in Fig. 7(a). The fluctuation of the output power (FOP) is less than 0.85% of the average power, indicative of a stable output power. The power variations from 600 min to 720 min are further enlarged, clearly revealing a weak fluctuation (less than 1.7 mW). The main reason for the small power instability may come from the fluctuations in pump laser and ambient temperature. In the case of high-power pumping and high-power output, the long-term power stability indicates that the fabricated YCDSF in this work has no obvious photodarkening effect, and the resultant suppression effect could be due to the incorporation of Y and Al elements in the YCDSF [16]. Long-term power stability is a very important indicator for the SFFLs used for coherent light beam combining and high-power seed light sources. The beam quality of the SFFL was recorded using a beam quality analyzer. The quality factors were calculated by the fitting of Gaussian function, yielding the same value of 1.016 in both the horizontal and vertical directions [Fig. 7(b)]. The waist widths of the lasing beam along the x and y axes are 586.56 μm and 584.73 μm, respectively, and their corresponding Rayleigh lengths are 258.29 mm and 256.65 mm. The inset in Fig. 7(b) shows the two-dimensional beam profile, whose energy distribution matches the standard Gaussian distribution. This confirms that output of the SFFL is a standard single transverse mode operation.

The performance of the SFFL in this work is compared with other phosphate- and silica-based all-fiber SFFLs, as shown in Table 1. First, the phosphate-based fibers [34,35] show a much higher Yb doping level than silica-based fibers, leading to a larger fiber gain coefficient and a higher slope efficiency in the constructed SFFLs. However, they suffer from relatively poor mechanical strengths over the YCDSFs. Besides, the SFFLs based on phosphates generally show a larger lasing threshold, for example, over 40 mW in Refs. [34,35], which may be accounted for from the mismatch occurring in the splicing between phosphate fibers and silica fibers. Compared with

Table 1. Summary of the All-Fiber DBR SFFLs Based on Different Gain Fibers

Fiber Type	Yb-Doped Phosphate Glass Fibers		Yb-Doped Silica Fiber (Fibercore, DF1100)		Yb-Doped Silica Fiber	YCDSF-1	YCDSF
Yb concentration (%, mass fraction)	18.30	15.20	<1.00	<1.00	/	4.80	5.66
Gain coefficient (dB/cm)	/	5.7 at 1064 nm	/	/	/	1.7 at 1064 nm	4.4 at 1030 nm
Gain fiber length (cm)	1.8	0.8	1.1	1.9	1.5	1.4	0.7
Slope efficiency (%)	38.6	75.4	27.0	28.0	/	18.5	34.9
Maximum output power (mW)	100.0	210.7	160.0	126.2	35.0	110.0	258.0
Threshold power (mW)	40	50	5	1.7	10	/	25
OSNR (dB)	61	65	/	/	65	80	79
Power stability	<0.10% at 8.0 h at 17 mW	0.50% at 1.0 h at 34 mW	1.30% at 1.0 h at 80 mW	0.54% at 0.5 h at 67 mW	<0.90% at 2.0 h	0.51% at 1.0 h at 110 mW	<0.85% at 13.0 h at 210 mW
Refs.	[34]	[35]	[36]	[37]	[38]	[13]	This work

phosphate gain fibers, although the YCDSF has a low gain coefficient, the SFFLs built on them present a better performance in slope efficiency and maximum output power. It has been long time that the Yb-doped silica-based fibers [36–38] made by MCVD methods have had limited Yb doping concentrations, resulting in a relatively low gain coefficient. Consequently, in order to generate a sufficiently high gain, a much longer gain fiber has to be integrated within the SFFL cavity to overcome the constraints. However, the longer the effective cavity of the laser, the smaller the longitudinal mode spacing [Fig. 4(b)]. As such, the method of utilizing the long gain fibers would inevitably deteriorate the stable SLM operation. In addition to this, it is likely that the single-frequency DBR fiber laser built in this way would also have the disadvantage in maximum output power, OSNR, and slope efficiency because of the low gain per unit length. As already discussed before, the accomplishment of the YCDSFs made using the melt-in-tube technique has greatly improved rare-earth ion doping in the fiber cores. Compared with YCDSF-1 [13], the YCDSF in this work has an enhancement in the Yb concentration, i.e., from 4.80% to 5.66% (mass fraction). As a consequence, the maximum output power and slope efficiency of the SFFL in this work are doubled, albeit the utilized length of YCDSF is only a half that of the YCDSF-1. Besides, the power fluctuation under long-term high-power conditions is rather small, due to the suppressed light darkening effect associated with the YCDSF. In short, the single-frequency DBR fiber laser based on the fabricated YCDSFs in this work has shown a significant improvement in performance.

The relative intensity noise (RIN) was examined at different pump powers, and in this case the used ESA had a resolution bandwidth of 30 Hz. As depicted in Fig. 8(a), the RIN spectrum at a given pump power is dominated by a sharp peak at the frequency of relaxation oscillation of the laser. As the pump power increases, the central frequency of the peak shifts toward higher frequencies, i.e., from 2 MHz at 310 mW to 3.6 MHz at 965 mW, whereas the peak intensity decreases from −98 dB/Hz to −110 dB/Hz correspondingly. At the highest frequency of 10 MHz, the RIN falls within the range of −135 dB/Hz to −138.7 dB/Hz under the tested pump power. To clearly reveal the RIN in the low-frequency region, the RIN

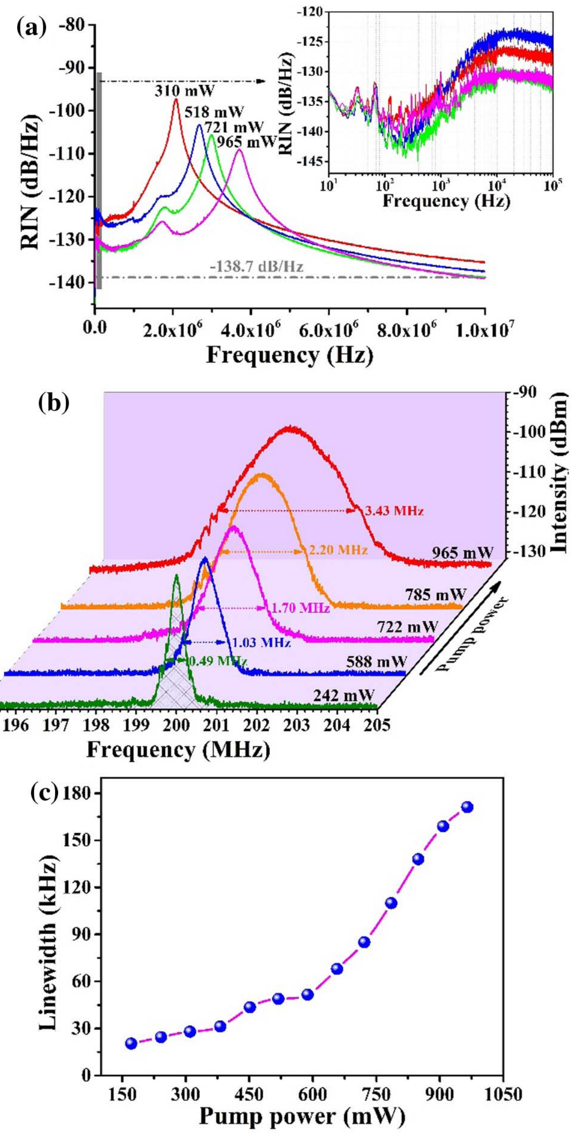

Fig. 8. Measured (a) relative intensity noise (RIN), (b) heterodyne signal, and (c) linewidth of the SFFL versus the pump power.

spectrum is plotted in the range of 10 Hz to 100 kHz and is shown as the inset in Fig. 8(a). In this graph, the RIN spectra appear as broad humps, all below −123 dB/Hz, within the range of 1 to 100 kHz, essentially due to the elevation of the associated relaxation oscillation frequency. A number of small peaks under 130 dB/Hz are also observed in the range from 10 Hz to 1 kHz, mainly originating from the ambient acoustics and vibrations, the power fluctuation of the pump laser, and the ASE of the Yb^{3+} ions [34]. With the increase of pump power, the RINs were almost overlapping, suggesting that the influence of ASE of the Yb^{3+} ions was small.

According to the delayed self-heterodyne method, the linewidth of the SFFL was studied, in which a 10 km long single fiber was used to provide a delay of 0.05 ms and a linewidth resolution of 15 kHz. During the measurement, a 200 MHz frequency shift was introduced using the AOM so as to avoid the interference of low-frequency signals, and the applied ESA had a sweep time of 0.69 s with a 30 Hz bandwidth resolution. Figure 8(b) shows these typical heterodyne signals with respect to the pump power. As can be seen from the figure, the 20 dB linewidth of the heterodyne signals gradually increases from 0.49 MHz at 242 mW to 1.7 MHz at 722 mW and 3.43 MHz at 965 mW. The linewidth of the laser can be estimated by dividing the 20 dB linewidth of the heterodyne signal by 20. A clear relationship between the linewidth and the pump power is also presented in Fig. 8(c). When the launched pump power rises from 170 to 965 mW, the measured linewidth increases from 20 to 171 kHz. A rapid increase in linewidth after 600 mW is also observed, which might be due to the significant heat accumulation in the YCDSFs. This is because that part of the pump light might not contribute to the stimulated transition process of Yb^{3+} ions, but rather than would be released in the form of heat [39]. The generated heat could modulate the refractive index of the YCDSF, causing linewidth broadening [40]. In general, the obtained linewidth of the laser in this work agrees with those of reported silica-based SFFLs [13,36], but it is broader than those of other phosphate-based SFFLs [10,34,35]. Further improvement can be realized by self-injection locking technology with passive optical feedback loops [41].

4. CONCLUSION

In summary, we have demonstrated an all-fiber DBR SFFL at 1030 nm based on an ultrashort YCDSF highly doped with 5.66% (mass fraction) Yb. The absorption, emission, and gain cross sections of the fabricated YCDSF are calculated. A stable single transverse and longitudinal mode operation has been accomplished with the DBR cavity based on a 0.7 cm long YCDSF. The SFFL built has a slope efficiency of 35% with an FOP of 0.85% within the examined duration over 10 h, showing the maximum output power of up to 258 mW. The OSNR of the laser is 79 dB with a beam quality of 1.016 in both the x and y axial directions. As the pump power increases, the measured RINs gradually decreases from −135 to −138.7 dB/Hz at 10 MHz, while the linewidth gradually increases from 20 to 171 kHz. The study suggests that the high-performance single-frequency DBR fiber lasers constructed from high-gain YCDSF could be applied as a seed source for a high-power fiber laser and detection source for the optical sensing.

Funding. National Key Research and Development Project (2020YFB1805800); National Natural Science Foundation of China (61520106014, 61675125, 61705126, 61735009); 111 Project (D20031); Shanghai Professional Technical Public Service Platform of Advanced Optical Waveguide Intelligent Manufacturing and Testing (19DZ2294000).

Acknowledgment. We are grateful to Profs. Hairun Guo, Liang Zhang, and Chengbo Mou at Shanghai University, China, for their help in data analysis and insightful discussion on the performance of the DBR SFFL.

Disclosures. The authors declare no conflicts of interest.

REFERENCES

1. H. R. Guo, M. Karpov, E. Lucas, A. Kordts, M. H. P. Pfeiffer, V. Brasch, G. Lihachev, V. E. Lobanov, M. L. Gorodetsky, and T. J. Kippenberg, "Universal dynamics and deterministic switching of dissipative Kerr solitons in optical microresonators," Nat. Phys. **13**, 94–102 (2017).
2. C. Dixneuf, G. Guiraud, Y. V. Bardin, Q. Rosa, M. Goeppner, A. Hilico, C. Pierre, J. Boullet, N. Traynor, and G. Santarelli, "Ultra-low intensity noise, all fiber 365 W linearly polarized single frequency laser at 1064 nm," Opt. Express **28**, 10960–10969 (2020).
3. F. Wellmann, M. Steinke, F. Meylahn, N. Bode, B. Willke, L. Overmeyer, J. Neumann, and D. Kracht, "High power, single-frequency, monolithic fiber amplifier for the next generation of gravitational wave detectors," Opt. Express **27**, 28523–28533 (2019).
4. C. Y. Qin, K. P. Jia, Q. Y. Li, T. Tan, X. H. Wang, Y. H. Guo, S. W. Huang, Y. Liu, S. N. Zhu, Z. D. Xie, Y. J. Rao, and B. C. Yao, "Electrically controllable laser frequency combs in graphene-fibre microresonators," Light Sci. Appl. **9**, 185 (2020).
5. C. Spiegelberg, J. H. Geng, Y. D. Hu, Y. Kaneda, S. B. Jiang, and N. Peyghambarian, "Low-noise narrow-linewidth fiber laser at 1550 nm (June 2003)," J. Lightwave Technol. **22**, 57–62 (2004).
6. O. V. Butov, A. A. Rybaltovsky, A. P. Bazakutsa, K. M. Golant, M. Y. Vyatkin, S. M. Popov, and Y. K. Chamorovskiy, "1030 nm Yb^{3+} distributed feedback short cavity silica-based fiber laser," J. Opt. Soc. Am. B **34**, A43–A48 (2017).
7. M. J. Yin, S. H. Huang, B. L. Lu, H. W. Chen, Z. Y. Ren, and J. T. Bai, "Slope efficiency over 30% single-frequency ytterbium-doped fiber laser based on Sagnac loop mirror filter," Appl. Opt. **52**, 6799–6803 (2013).
8. Z. K. Wang, J. M. Shang, K. L. Mu, Y. J. Qiao, and S. Yu, "Single-longitudinal-mode fiber laser with an ultra-narrow linewidth and extremely high stability obtained by utilizing a triple-ring passive subring resonator," Opt. Laser Technol. **130**, 106329 (2020).
9. Y. Kaneda, C. Spiegelberg, J. H. Geng, Y. D. Hu, T. Luo, J. F. Wang, and S. B. Jiang, "200-mW, narrow-linewidth 1064.2-nm Yb-doped fiber laser," in *Conference on Lasers and Electro-Optics/International Quantum Electronics Conference and Photonic Applications Systems Technologies* (Optical Society of America, 2004), paper CThO3.
10. S. H. Xu, Z. M. Yang, W. N. Zhang, X. M. Wei, Q. Qian, D. D. Chen, Q. Y. Zhang, S. X. Shen, M. Y. Peng, and J. R. Qiu, "400 mW ultrashort cavity low-noise single-frequency Yb^{3+}-doped phosphate fiber laser," Opt. Lett. **36**, 3708–3710 (2011).
11. S. L. Kang, T. Qiao, X. J. Huang, C. S. Yang, X. F. Liu, J. R. Qiu, Z. M. Yang, and G. P. Dong, "Enhanced CW lasing and Q-switched pulse generation enabled by Tm^{3+}-doped glass ceramic fibers," Adv. Opt. Mater. **9**, 2001774 (2020).
12. G. W. Tang, G. Q. Qian, W. Lin, W. L. Wang, Z. G. Shi, Y. Yang, N. L. Dai, Q. Qian, and Z. M. Yang, "Broadband 2 μm amplified spontaneous emission of Ho/Cr/Tm:YAG crystal derived all-glass fibers for

mode-locked fiber laser applications," Opt. Lett. **44**, 3290–3293 (2019).
13. Z. J. Liu, Y. Y. Xie, Z. H. Cong, Z. G. Zhao, Z. X. Jia, C. Z. Li, G. S. Qin, S. Wang, X. B. Gao, X. B. Shao, and X. Y. Zhang, "110 mW single-frequency Yb: YAG crystal-derived silica fiber laser at 1064 nm," Opt. Lett. **44**, 4307–4310 (2019).
14. X. C. Guan, Q. L. Zhao, W. Lin, T. Y. Tan, C. S. Yang, P. F. Ma, Z. M. Yang, and S. H. Xu, "High-efficiency and high-power single-frequency fiber laser at 1.6 μm based on cascaded energy-transfer pumping," Photon. Res. **8**, 414–420 (2020).
15. P. D. Dragic, J. Ballato, T. Hawkins, and P. Foy, "Feasibility study of Yb: YAG-derived silicate fibers with large Yb content as gain media," Opt. Mater. **34**, 1294–1298 (2012).
16. C. Z. Li, Z. X. Jia, Z. H. Cong, Z. J. Liu, X. Y. Zhang, G. S. Qin, and W. P. Qin, "Gain characteristics of ytterbium-doped SiO_2–Al_2O_3–Y_2O_3 fibers," Laser Phys. **29**, 055804 (2019).
17. Y. F. Wang, Y. M. Zhang, J. K. Cao, L. P. Wang, X. L. Peng, J. P. Zhong, C. S. Yang, S. H. Xu, Z. M. Yang, and M. Y. Peng, "915 nm all-fiber laser based on novel Nd-doped high alumina and yttria glass @ silica glass hybrid fiber for the pure blue fiber laser," Opt. Lett. **44**, 2153–2156 (2019).
18. Y. M. Zhang, G. Q. Qian, X. S. Xiao, X. L. Tian, X. Q. Ding, Z. J. Ma, L. Y. Yang, H. T. Guo, S. H. Xu, Z. M. Yang, and J. R. Qiu, "The preparation of yttrium aluminosilicate (YAS) glass fiber with heavy doping of Tm^{3+} from polycrystalline YAG ceramics," J. Am. Ceram. Soc. **101**, 4627–4633 (2018).
19. S. P. Zheng, J. Li, C. L. Yu, Q. L. Zhou, and D. P. Chen, "Preparation and characterizations of Nd:YAG ceramic derived silica fibers drawn by post-feeding molten core approach," Opt. Express **24**, 24248–24254 (2016).
20. Y. M. Zhang, G. Q. Qian, X. S. Xiao, X. L. Tian, Z. Chen, J. P. Zhong, Z. J. Ma, H. T. Guo, S. H. Xu, Z. M. Yang, and J. R. Qiu, "A yttrium aluminosilicate glass fiber with graded refractive index fabricated by melt-in-tube method," J. Am. Ceram. Soc. **101**, 1616–1622 (2018).
21. P. Dragic, P. C. Law, J. Ballato, T. Hawkins, and P. Foy, "Brillouin spectroscopy of YAG-derived optical fibers," Opt. Express **18**, 10055–10067 (2010).
22. P. D. Dragic, Y. S. Liu, J. Ballato, T. Hawkins, and P. Foy, "YAG-derived fiber for high-power narrow-linewidth fiber lasers," Proc. SPIE **8237**, 82371E (2012).
23. S. P. Zheng, J. Li, C. L. Yu, Q. L. Zhou, L. L. Hu, and D. P. Chen, "Preparation and characterizations of Yb:YAG-derived silica fibers drawn by on-line feeding molten core approach," Ceram. Int. **43**, 5837–5841 (2017).
24. Y. M. Zhang, W. W. Wang, J. Li, X. S. Xiao, Z. J. Ma, H. T. Guo, G. P. Dong, S. H. Xu, and J. R. Qiu, "Multi-component yttrium aluminosilicate (YAS) fiber prepared by melt-in-tube method for stable single-frequency laser," J. Am. Ceram. Soc. **102**, 2551–2557 (2019).
25. Y. Y. Xie, Z. J. Liu, Z. H. Cong, Z. G. Qin, S. Wang, Z. X. Jia, C. Z. Li, G. S. Qin, X. B. Gao, and X. Y. Zhang, "All-fiber-integrated Yb:YAG-derived silica fiber laser generating 6 W output power," Opt. Express **27**, 3791–3798 (2019).
26. Y. Wan, J. X. Wen, Y. H. Dong, C. Jiang, M. Jia, F. Z. Tang, N. Chen, Z. W. Zhao, S. J. Huang, F. F. Pang, and T. Y. Wang, "Exceeding 50% slope efficiency DBR fiber laser based on a Yb-doped crystal-derived silica fiber with high gain per unit length," Opt. Express **28**, 23771–23783 (2020).
27. H. Noel, M. Fokine, Y. Franz, T. Hawkins, M. Jones, J. Ballato, A. C. Peacock, and U. J. Gibson, "CO_2 laser-induced directional recrystallization to produce single crystal silicon-core optical fibers with low loss," Adv. Opt. Mater. **4**, 1004–1008 (2016).
28. D. E. McCumber, "Einstein relations connecting broadband emission and absorption spectra," Phys. Rev. **136**, A954–A957 (1964).
29. F. B. Slimen, S. X. Chen, J. Lousteau, Y. M. Jung, N. White, S. Alam, D. J. Richardson, and F. Poletti, "Highly efficient Tm^{3+} doped germanate large mode area single mode fiber laser," Opt. Mater. Express **9**, 4115–4125 (2019).
30. P. Barua, E. H. Sekiya, K. Saito, and A. J. Ikushima, "Influences of Yb^{3+} ion concentration on the spectroscopic properties of silica glass," J. Non-Cryst. Solids **354**, 4760–4764 (2008).
31. W. Zhang, J. T. Liu, G. Y. Zhou, C. M. Xia, J. L. Wu, Y. Chen, X. L. Cang, and Z. Y. Hou, "Analysis on the optical properties for the ytterbium doped silica glasses prepared by laser sintering technology," Opt. Quantum Electron. **49**, 27 (2017).
32. H. X. Li, J. Lousteau, W. N. MacPherson, X. Jiang, H. T. Bookey, J. S. Barton, A. Jha, and A. K. Kar, "Thermal sensitivity of tellurite and germanate optical fibers," Opt. Express **15**, 8857–8863 (2007).
33. Y. O. Barmenkov, D. Zalvidea, S. Torres-Peiró, J. L. Cruz, and M. V. Andrés, "Effective length of short Fabry-Perot cavity formed by uniform fiber Bragg gratings," Opt. Express **14**, 6394–6399 (2006).
34. S. H. Xu, C. Li, W. N. Zhang, S. P. Mo, C. S. Yang, X. M. Wei, Z. M. Feng, Q. Qian, S. X. Shen, M. Y. Peng, Q. Y. Zhang, and Z. M. Yang, "Low noise single-frequency single-polarization ytterbium-doped phosphate fiber laser at 1083 nm," Opt. Lett. **38**, 501–503 (2013).
35. Z. M. Feng, S. P. Mo, S. H. Xu, X. Huang, Z. R. Zhong, C. S. Yang, C. Li, W. N. Zhang, D. D. Chen, and Z. M. Yang, "A compact linearly polarized low-noise single-frequency fiber laser at 1064 nm," Appl. Phys. Express **6**, 052701 (2013).
36. B. Sun, J. Jia, J. Huang, X. Q. Zhang, and J. T. Bai, "A 1030 nm single-frequency distributed Bragg reflector Yb-doped silica fiber laser," Laser Phys. **27**, 105105 (2017).
37. B. Sun, X. Q. Zhang, and J. Jia, "Single-frequency fiber laser at 1030 nm based on gain bandwidth compression," Laser Phys. Lett. **16**, 065101 (2019).
38. W. Guan and J. R. Marciante, "Single-polarisation, single-frequency, 2 cm ytterbium-doped fibre laser," Electron. Lett. **43**, 558–560 (2007).
39. Y. F. Wang, J. M. Wu, Q. L. Zhao, W. W. Wang, J. Zhang, Z. M. Yang, S. H. Xu, and M. Y. Peng, "Single-frequency DBR Nd-doped fiber laser at 1120 nm with a narrow linewidth and low threshold," Opt. Lett. **45**, 2263–2266 (2020).
40. G. P. Agrawal, "Line narrowing in a single-mode injection laser due to external optical feedback," IEEE J. Quantum Electron. **20**, 468–471 (1984).
41. Z. P. Huang, H. Q. Deng, C. S. Yang, Q. L. Zhao, Y. F. Zhang, Y. N. Zhang, Z. M. Feng, Z. M. Yang, M. Y. Peng, and S. H. Xu, "Self-injection locked and semiconductor amplified ultrashort cavity single-frequency Yb^{3+}-doped phosphate fiber laser at 978 nm," Opt. Express **25**, 1535–1541 (2017).